

Modal testing and finite element model updating of full-scale hybrid timber-concrete building

Blaž Kurent^a, Wai Kei Ao^{b,*}, Aleksandar Pavic^{c,d,e}, Fernando Pérez^f, Boštjan Brank^a

^a Faculty of Civil and Geodetic Engineering, University of Ljubljana, Ljubljana, Slovenia

^b The Hong Kong Polytechnic University, Civil and Environmental Engineering, Hung Hom, Kowloon, Hong Kong

^c Department of Engineering, University of Exeter, Exeter, UK

^d Faculty of Civil Engineering, The University "Union - Nikola Tesla", Belgrade, Serbia

^e Full Scale Dynamics Ltd, Colyton, UK

^f Smith and Wallwork Engineers, 50 St Andrew Street, Cambridge CB2 3AH, UK

ARTICLE INFO

Keywords:

Modal testing
Timber building
Hybrid building
Model updating
Cross-laminated timber
Finite element model
Lateral vibrations in service

ABSTRACT

Serviceability of tall timber and hybrid timber buildings under wind-induced vibrations has become their leading design criterion. Accurate finite element models for predicting their modal properties are crucial for designing buildings that satisfy the current serviceability criteria. It is a challenge for structural engineers to decide what to include in the structural modelling. This is because elements that are typically considered non-structural (partition walls, plasterboards, screed, façade, etc.) have been shown to act structurally and can significantly influence the modal properties of timber buildings.

This paper discusses the importance of including certain entities in finite element models of timber and hybrid timber buildings. A case study of a 5-storey hybrid timber-concrete building with masonry cladding is presented. Full-scale in-situ dynamic tests were performed on the building, using forced vibration testing with a shaker. Frequency-response-function-based modal identification resulted in 3 modes of vibration, identifying natural frequencies, mode shapes and damping ratios. A detailed finite element model was developed that estimated the measured natural frequencies with an error of slightly more than 11%.

With an extensive sensitivity analysis was found that modelling of the foundation, the effect of the adjacent abutting building in contact, and the masonry cladding was needed. After model updating, it was found that the shear stiffness of CLT walls was initially underestimated, concluding that non-structural elements such as plasterboards and partition walls might influence the dynamic properties of this hybrid timber-concrete building.

1. Introduction

The present climate emergency requires a serious and fast rethinking of how the construction sector operates worldwide. The UN Environment and International Energy Agency [1] estimates that the total building floor area will double by 2060 with 230bn m² of new floors. This is equivalent to adding one Paris to the planet Earth every week for the next 38 years. Considering such a huge intensity of construction, it should not be surprising that the built environment currently generates 39% of 42 GtCO₂e of all annual emissions in the world. Of these 28% is pertinent to the buildings' construction and operation and 11% to the rest of the construction industry. This is not surprising knowing that just cement and steel productions currently generate 14–15% of all global CO₂ emissions. So, a good estimate [2] is that 10% of all worldwide

annual emissions i.e., a staggering 4.2 GtCO₂e is due to – structural engineering decision-making.

The key structural engineering decision when constructing a building is the selection of the construction material, and the choice is currently quite limited and dominated by concrete and steel. However, timber is a rare construction material that is renewable and has the capacity of sequestering CO₂ rather than generating it. Trees on average absorb twice as much CO₂ as they emit every year [3].

This is why timber is increasingly being considered as a replacement for as much steel and concrete as possible. Practical constructability considerations will normally require some use of concrete and steel in buildings (for example, for concrete foundations, floor screed, vertical elevator and staircase cores, as well as the steel-made connections, ties and braces). This, therefore, gave rise to hybrid timber structures which

* Corresponding author.

E-mail address: waikei.ao@polyu.edu.hk (W.K. Ao).

<https://doi.org/10.1016/j.engstruct.2023.116250>

Received 13 December 2022; Received in revised form 28 April 2023; Accepted 30 April 2023

Available online 12 May 2023

0141-0296/© 2023 The Authors. Published by Elsevier Ltd. This is an open access article under the CC BY license (<http://creativecommons.org/licenses/by/4.0/>).

exploit the best features of timber as a structural material working together with steel, concrete and polymers, as appropriate.

Apart from being renewable and able to sequester carbon, other important to remember features of timber in buildings are its light weight and reduced stiffness compared with concrete and steel [4]. However, the low mass also means that vibration serviceability due to wind-induced lateral sway has become a de-facto governing design criterion for multi-storey hybrid timber buildings. This means it is dictating the size and shape and therefore environmental and financial cost of such structures [5].

Vibration serviceability requires a calculation of the lateral sway which in turn requires modal properties of the structure: natural frequencies, modal damping ratios, mode shapes and modal masses [6]. Two or more materials, working together in any hybrid structure is inherently difficult to model due to uncertain nature connections between the materials. This attracted significant research interest specifically for hybrid structures to improve understanding and modelling of such structures. This is particularly so for hybrid timber structures and their dynamic behaviour due to the previously mentioned beneficial effects of timber and lateral sway governing the design of such structures.

The vast majority of the relevant published papers used ambient vibration testing (AVT) to estimate experimentally the as-built natural frequencies, modal damping ratios and mode shapes. The output-only AVT generally yields a lower number of identified modes of vibration with modal properties of lower quality and reliability, compared with the input–output frequency response function (FRF) based modal testing [7].

Tulebekova et al. [8] reported AVT results identifying five modes of vibration of Mjøstårnet, currently the highest timber building in the world. A finite element (FE) model was developed and updated manually to match the FE and experimental modal properties. This yielded the rigidity of the key connections throughout the building. Aloisio et al. [9] reported results of AVT used on an 8-storey cross-laminated timber (CLT) building. They managed to identify experimentally three modes. No attempt was made to develop and update a detailed FE model based on the measured modal properties. Reynolds et al. [10] performed AVT on a 7-storey CLT-only building which featured an absolute minimum of concrete and steel. They measured on two separate occasions during entirely different construction phases and – surprisingly – concluded that the fundamental natural frequency decreased with adding the non-structural components, such as walls and façade.

For standard steel and concrete multi-storey buildings, adding such non-structural components normally increases the natural frequency [11–13]. Other researchers [14] reached the same conclusion through testing a 3-storey OSB sheathed light-frame timber residential building with timber-concrete composite slabs. Measurements were carried out in two construction phases: first without and then with non-structural façade and partitions. They employed two full-scale dynamic testing techniques: AVT and forced vibration testing (FVT) but without measuring the input–output relationship between the measured force and the corresponding response. A hydraulic shaker was used for the FVT which allowed excitation with a controlled forcing amplitude and hence a study of an amplitude-dependent behaviour of the test structure. Significantly, this study found that (i) non-structural components increased the natural frequencies, (ii) when increasing the amplitude of excitation, the natural frequencies reduce and the stiffening effect of the non-structural elements decreased, and (iii) damping significantly increased with amplitude.

More than 20 years ago Ellis & Bougard [15] tested a laboratory-based 6-storey light timber-framed building featuring brick wall cladding. AVT and response-only sinusoidal FVT was carried out using a horizontal rotating-mass shaker. Being laboratory-based, it was possible to carefully study several construction phases. It was found that there was a significant increase in stiffness after adding plasterboard walls and stairs. Moreover, a very significant additional increase in natural

frequency resulting from the increase in the stiffness that was greater than the increase in the mass was found after the construction of a masonry cladding. However, no FE modelling accompanied this work and the building featured a standard timber frame and not modern CLT.

Reynolds et al. [16] studied two 5-storey timber-concrete hybrid buildings. The two buildings had the same layout, but – quite interestingly – different timber structural systems. One building utilised light timber frame and the other CLT while both had a concrete core for the staircase. The AVT managed to identify the first 3 modes for each building revealing similar dynamic properties of two structural systems, which was the most significant finding.

Another 4-storey timber-concrete hybrid building (featuring glued laminated timber beams, CLT slabs and concrete core) was tested [17]. A three-year AVT monitoring programme identified a significant 10% seasonal variation in the fundamental natural frequency due to humidity. The higher moisture content yielded stiffening and higher natural frequency.

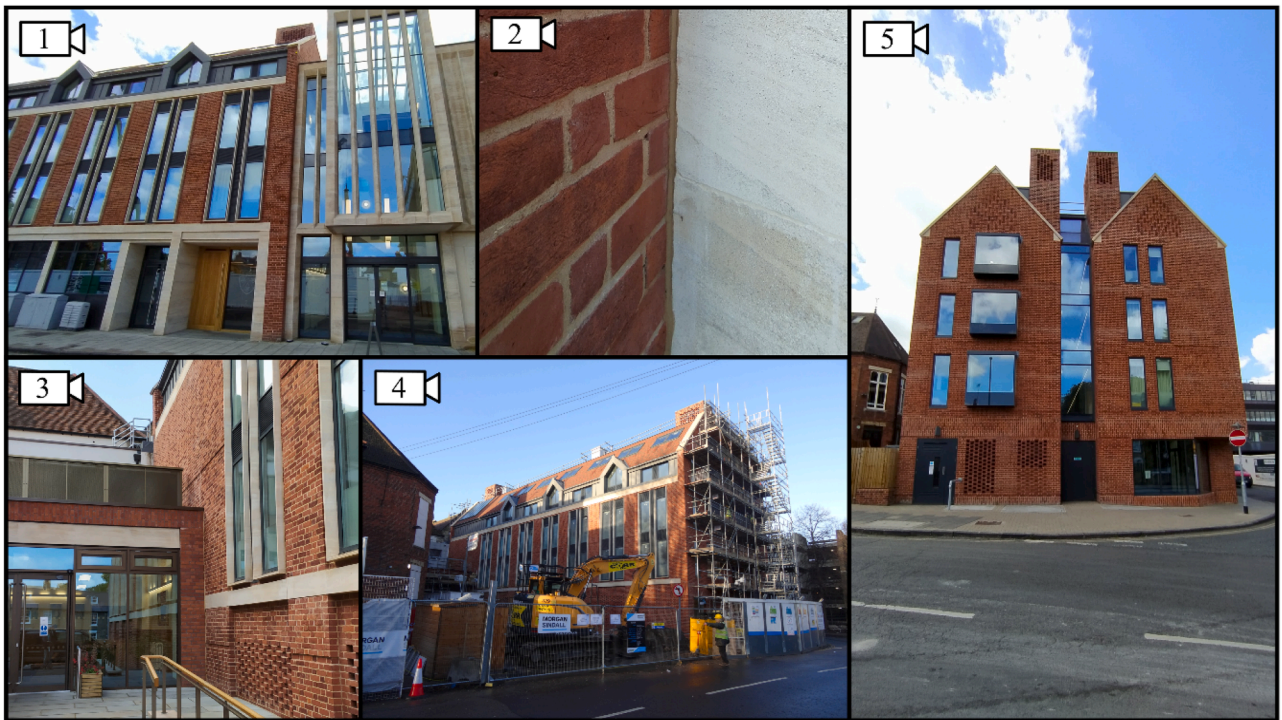
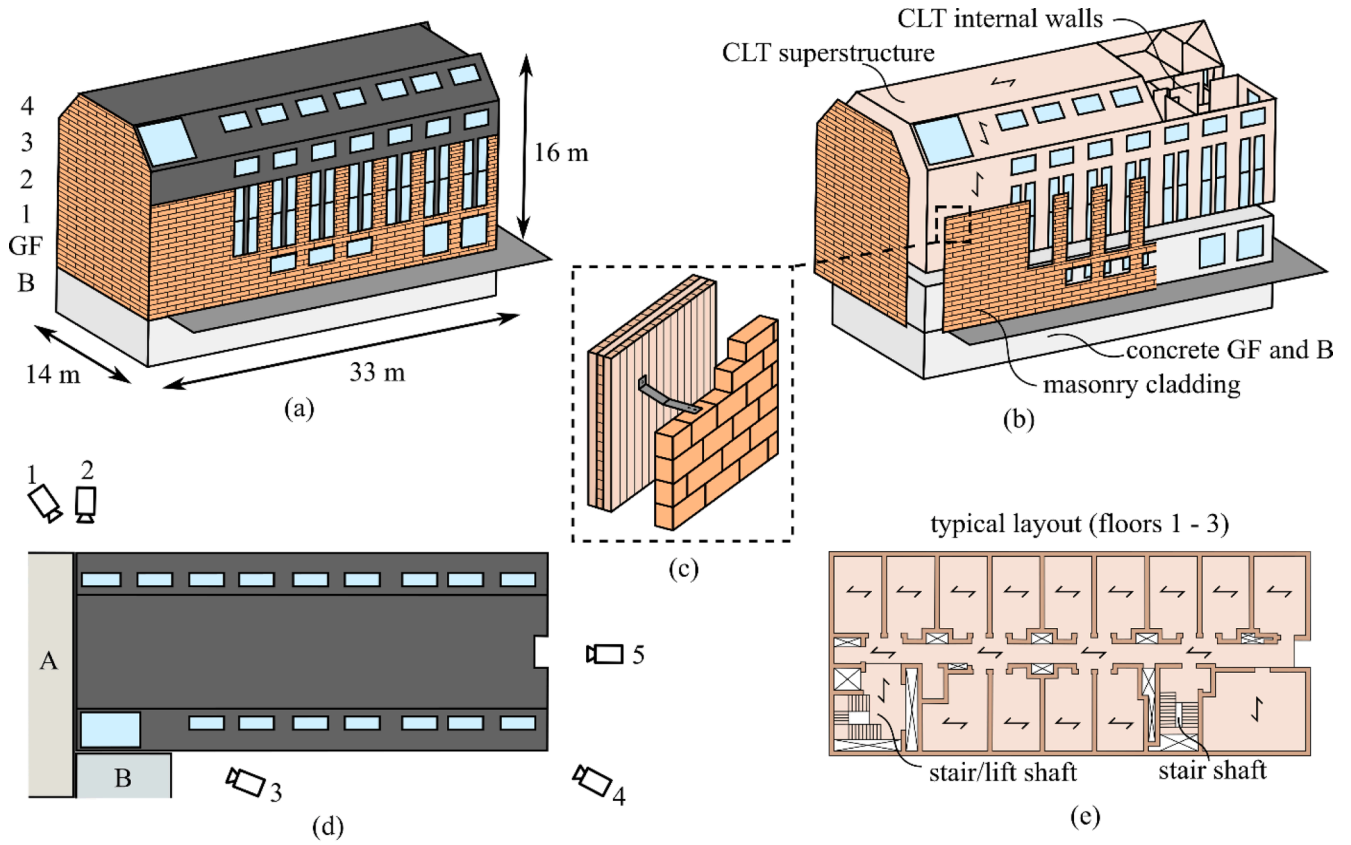
In virtually all investigations mentioned and done by others reviewed by the authors of this paper, an output-only AVT was used as the principal method for dynamic testing of full-scale structures. On the other hand, an input–output FVT is a standard method of dynamic testing of full-scale mechanical and aerospace structures, such as cars and aircraft. The reason for this is that relative to AVT, the FVT-based modal testing yields more experimentally measured modes with properties, in particular damping, mode shapes and modal masses, that are of considerably better quality [18,19].

The authors of this paper have previously analysed experimentally and analytically a 7-storey CLT building using FVT, identifying not less than eight modes with natural frequencies as high as 8 Hz, which is practically impossible to measure using AVT [20]. Six modes were well matched with a detailed FE model, which was updated using Bayesian model updating [21]. It has been found that the lateral stiffness of the building is higher than offered by CLT walls with the shear modulus proposed by their producers. It has been concluded that non-structural components contribute to the overall lateral stiffness of the building and steel connections between walls and floors do not reduce stiffness significantly (or not at all). The conclusions of the study were case-specific due to a large variety of structural and non-structural elements that are used in timber and hybrid timber buildings. The aim of this paper is to replicate the results on a building with different shape and different structural systems. A hybrid timber-concrete building with masonry cladding is modelled in detail and tested with FVT. The FE model is updated with the aim of identifying initial modelling error and finding the influence of the non-structural elements on the serviceability dynamic behaviour.

The structure of the paper is as follows. Section 2 presents the studied building with relevant information about its structural systems. Section 3 describes the initial FE model that was built prior to modal testing. Used material properties and other adopted assumptions are presented. Then modal testing procedure, setup and the results of modal testing are described in Section 4. In Section 5, several attempts are made to improve the FE model by changing different model parameters. Their effects are presented and the rationale for selecting the set of parameters for model updating is explained. The results of model updating and the discussion of the findings then follow. Finally, concluding remarks are given in Section 6.

2. Structural description

The full-scale building structure tested is a new student accommodation from Trinity College, Cambridge, situated on Round Church Street (Fig. 1). Its overall dimensions are shown in Fig. 1a. It has one storey basement (B), a ground floor (GF) made of concrete plus four floors (1–4) made of CLT floor slabs and load-bearing CLT walls (Fig. 1b). The structure of the building could be classified as a mixed timber/concrete building, according to [22]. A significant proportion of



(f)

Fig. 1. Information about Trinity building: (a) dimensions of the building, (b) structural systems, (c) typical connection between CLT structure and masonry cladding, (d) location of the two adjacent buildings, (e) typical layout of CLT walls within the storey, and (f) photographs of the hybrid timber-concrete building tested.

the façade is comprised of a 100 mm thick self-supporting masonry cladding, horizontally connected to the CLT structure with ties, as shown in Fig. 1c. The masonry cladding is not considered to take any structural vertical or lateral loads. The building is located in a tight urban environment. At the South-West end of the building, two adjacent buildings (denoted as A and B in Fig. 1d) abut against it while the other end is free. They were constructed simultaneously, but they are structurally independent. The cladding elements of the abutting buildings are notionally connected, however, no documentation about possible steel ties between them was obtained. Fig. 1f shows photographs of the building from different angles. Adjacent building A is shown in photograph 1 with a closer look at the contact between the buildings in photograph 2. Contact with the adjacent building B is shown in photograph 3.

The basement of the building is constructed using steel sheet piling and a 600 mm thick basement concrete raft providing the main foundation for the building. The concrete walls of the basement as well as of the GF are 200 mm thick. Above the basement, there is a 300 mm thick GF slab and a 450 mm thick first-floor concrete transfer slab that provides support for the rest of the CLT superstructure. Internal cross walls create 13 student rooms and a community kitchen in a typical layout (Fig. 1e) of floors 1–3 and a slightly different layout on the top-level floor. All CLT walls are load-bearing, generally of thickness between 90 and 140 mm (typically 120 mm), with the lift shaft featuring a 200 mm CLT wall at one side. CLT floor slabs are 140 mm or 160 mm thick (in the kitchen 180 mm due to the greater floor span). The roof, which is supported by the internal and external CLT walls, is made of 140 mm and 180 mm panels. For the most part, panels with 5 layers are used, except for the 90 mm walls, where panels with 3 layers are used. C24 grade spruce panels of producer KLH are chosen. The narrow edges of the lamellae are glued, however, the performance of the glue is not controlled nor guaranteed.

Over each floor slab, approximately 25 mm thick sound insulation panels are installed, following a 65 mm thick layer of screed. Slabs are finished with wood flooring.

Based on the drawings and specifications of the materials, the total mass of the above-ground structure is about 2 000 t. Not surprisingly, almost half of it is concrete (900 t), then CLT (250 t), masonry (130 t), and screed (300 t). The rest of the building mass consists of non-structural elements (such as plasterboard wall lining, insulation, windows, doors, installations, etc.).

3. Initial FE model

An initial FE model was developed to facilitate the full-scale modal testing in terms of instrumentation and, in particular, the location of the excitation shakers, (see Section 4). The FE modelling assumptions and simplifications made have been:

- Only the structure above the ground was modelled (i.e. the basement was not modelled).
- Building elements assumed to have stiffness were concrete walls and floors, all CLT walls and floors, the CLT roof and the masonry cladding.
- Details smaller than 0.5 m (i.e. small holes, small CLT panels, slightly displaced walls...) were simplified or neglected.
- Windows and doors were modelled only as openings.
- Stairs were neglected and the floor slab was extended over the elevator and stair shafts.
- The ground floor slab was assumed to be rigidly constrained by fixing all displacements over the whole of its surface.
- All connections between adjoining elements were assumed to be rigid.
- External walls in contact with the abutting buildings were left unconstrained.

For all CLT and concrete walls and slabs, ANSYS SHELL181 element was used. Over the areas, where masonry cladding is present, an additional layer to SHELL181 elements is included, modelling masonry cladding as tightly bonded with CLT and concrete walls underneath. All concrete columns were modelled using ANSYS BEAM188 element. For concrete and masonry, an isotropic material model was adopted, whereas the orthotropic material model was used to model CLT panels. The key material properties were taken from the published literature, see Table 1. For CLT panels, the first-order shear-deformation shell theory for composite laminates was applied (see e.g. [23] and references therein) to get a shell constitutive matrix. The theory assumes an ideal bond between the CLT layers and an ideal bond between the boards in a single CLT layer. The stiffness of shell elements modelling CLT panels was further computed in a standard manner by using the default locking remedies incorporated in SHELL181.

For each storey, the mass of all the CLT (or concrete) floor slabs and the attached non-structural elements (screed, insulation, hardwood flooring, ceiling plasterboard, etc.) was calculated and uniformly distributed over shell elements modelling those floor slabs. Similarly, the mass of all the load-bearing CLT walls (or concrete walls in GF) together with non-structural elements (insulation, plasterboards, partition walls, etc.) was calculated and uniformly distributed over all the walls within each storey. The mass of the masonry cladding was distributed locally only over the elements where it was present. Finally, the mass of all the structural and non-structural elements of the roof was distributed uniformly over the whole surface of the roof.

The analysis of the convergence of the first three calculated natural frequencies is shown in Fig. 2. It was used to select an appropriate FE mesh size for model updating. The error was estimated as a relative difference from the nominally ‘most accurate’ FE model featuring 3 million nodes. A mesh size of 0.2 m (i.e. an FE model with 140 000 nodes) was found to be a good compromise between the speed and accuracy for the computationally expensive model updating procedure, with maximum error in the calculated natural frequency of well below 1%.

The first three modes of vibration found by the initial FE model are shown in Fig. 3, with their respective natural frequencies and unity-scaled modal masses. Mode 1 is a bending mode, while modes 2 and 3 are a combination of bending and torsion, probably caused by the lack of symmetry in the distribution of the horizontal stiffness throughout the building, driven mainly by the elevator and staircase CLT cores. Considering the distribution of the load-bearing CLT walls shown in Fig. 1d, the shape of the fundamental mode is logical as it seemingly bends the less stiff longer direction of the building.

4. Testing

An input–output modal testing (MT), or experimental modal analysis (EMA), was used to experimentally estimate the modal properties of the test structure [27,28]. This is an unusual type of dynamic testing of full-

Table 1
Adopted material properties for structural systems.

Concrete C30/37 [24]	Isotropic material model: $E = 33\,000\text{ MPa}$ $\nu = 0.2$ $\rho = 2\,500\text{ kg/m}^3$
CLT panel [25]	Orthotropic material model: $E_1 = 12\,000\text{ MPa}$ $E_2 = 450\text{ MPa}$ $G_{12} = G_{13} = 500\text{ MPa}$ $G_{23} = 50\text{ MPa}$ $\nu_{12} = 0.3$ $\rho = 500\text{ kg/m}^3$
Masonry [26]	Isotropic material model: $E = 6\,300\text{ MPa}$ $G = 0.4 * E_p = 2\,200\text{ kg/m}^3$

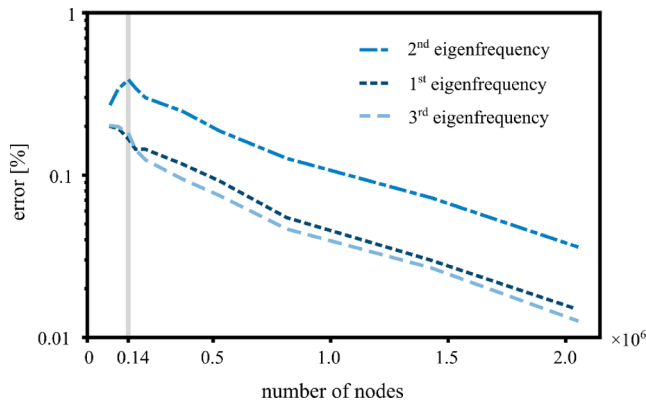


Fig. 2. Convergence analysis. Error is defined as a relative difference from the reference model with 3 million nodes.

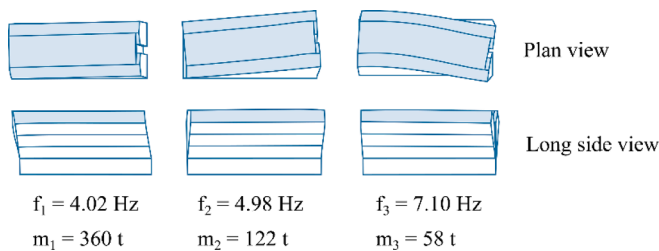


Fig. 3. The first three calculated modes of vibration by the initial FE model.

scale buildings as output-only ambient vibration testing (AVT), also known as operational modal analysis, is normally used [29–31]. However, MT where both the excitation force and the corresponding dynamic response are measured simultaneously with the aim of experimentally estimating and curve fitting the structure's FRF is a much more powerful tool where both the excitation force and the corresponding dynamic response are measured simultaneously.

For decades MT has traditionally dominated aerospace and automotive sectors whereas AVT has been very much used in experimental dynamic testing of large civil engineering structures. This is even though AVT has, by its very nature and due to its underpinning assumptions [32–36,29], rather inferior performance as to its quality of modal parameters relative to MT. MT has not been popular in the dynamic testing measuring sway modes of large civil engineering structures mainly due to the:

- logistical and practical difficulties of MT in measuring simultaneously the force and the corresponding vibration levels throughout the height of a real large scale building; and
- conundrum in MT of exciting the large structure with a measured force large enough so that the response to it can be measured simultaneously while the force is also not large enough to cause local damage at the point where it is imparted into the structure.

Testing was performed in December 2020, when the building was in the final stages of construction with the majority of structural and non-structural elements in place (a great part of the building already being furnished). A detailed description of the MT system used for this building is described elsewhere [37,38,18]. Fig. 4 (a-c) shows the elements of the experimental hardware. The MT test grid throughout the whole building is shown in Fig. 4d and the positioning of the three shakers and relevant test points on the 3rd floor is shown in Fig. 4e. The point acceleration FRF [27,28] was therefore measured on the 3rd floor.

There were 11 test points with two orthogonal degrees of freedom (x and y directions, Fig. 4e) measured at every test point. Nine OCXO [27]

4-channel data loggers were used in conjunction with twenty Honeywell QA 750 uniaxial force-balanced accelerometers [39] and five Japan Aviation Electronics (JAE) JA-70SA triaxial MEM accelerometers [40].

Two single-input multiple-output [27,28] modal tests were conducted using three APS400 [41] electrodynamic shakers positioned. The first test had shakers exciting the structure in the x direction and the second in the y direction. This yielded two rows of the FRF matrix which were possible to curve fit simultaneously using multiple references i.e. multiple-input multiple-output (MIMO) FRF-curve fitting algorithm [18]. This also provided an opportunity to check the quality of the FRF measurements by a reciprocity check [38]. Fig. 4f shows the results of such a check indicating, for a 2 000 t building, reasonable quality of the measured FRFs in the most important frequency range up to 10 Hz. Finally, Fig. 4f shows the results of a MIMO curve fitting indicating the reasonable quality of the fitted models considering the noisiness of the FRF moduli due to low signal-to-noise ratio when the three shakers with the maximum total horizontal force below 1 kN try to excite this 2 000 t building.

Three modes of vibration have been identified by MIMO curve-fitting of all 44 measured FRFs. The first two are bending modes and the third is a torsion mode. Their modal properties are presented in Table 2 and the realised mode shapes are shown in Fig. 5a. Damping ratios are similar to what has previously been identified for a CLT building [37]. By comparing these results with the calculated modal properties for the first three modes of vibration using the initial FE model (Table 2 and Fig. 5b), it can be seen that the best engineering judgement used to develop the initial FE model yielded some reasonable estimates. The sequence of mode shapes seems to be correct, but with some discrepancies in the natural frequencies which will be addressed through the FE model updating that follows.

5. Model updating

Quantities of interest that were predicted with the FE model and were later experimentally obtained are the first three natural frequencies and mode shapes. The discrepancy between the model and experiments is measured with a relative error of natural frequency:

$$\text{err}_{i,\text{freq}} = \frac{f_{i,\text{FE}} - f_{i,\text{exp}}}{f_{i,\text{exp}}}, \quad (1)$$

where $f_{i,\text{FE}}$ is the i -th natural frequency of the FE model and $f_{i,\text{exp}}$ the i -th natural frequency that was obtained from the experiments. For the measure of mode shape matching a modal assurance criterion (MAC) [42] was used:

$$\text{MAC}_i = \frac{|\Phi_{i,\text{FE}}^T \Phi_{i,\text{exp}}|^2}{(\Phi_{i,\text{FE}}^T \Phi_{i,\text{FE}})(\Phi_{i,\text{exp}}^T \Phi_{i,\text{exp}})}, \quad (2)$$

Where $\Phi_{i,\text{FE}}$ is the i -th eigenvector of the FE model and $\Phi_{i,\text{exp}}$ the i -th eigenvector that was obtained from the experiments. The assumption of realised eigenvectors [43] and the assumption of the same ordering of modes in the FE model and experiments were made. A MAC value of 1 suggests a strong correlation between mode shapes, whereas a MAC value of 0 suggests no correlation. Ideally, MAC values should be close to 1 to say that modes are matching. Fig. 6 shows how well the initial FE model matches the experiments.

5.1. Objective

Different current comfort criteria used for wind-induced vibration [44] require an estimate of the fundamental frequency. The initial FE model presented in Section 3 offers a good estimate for this purpose. A comparison of the initial FE model with the experiments shows that the model underestimated the first natural frequency by 10 %. Eurocode 1 [45] offers an estimation of the first natural frequency as $46/h$, where h

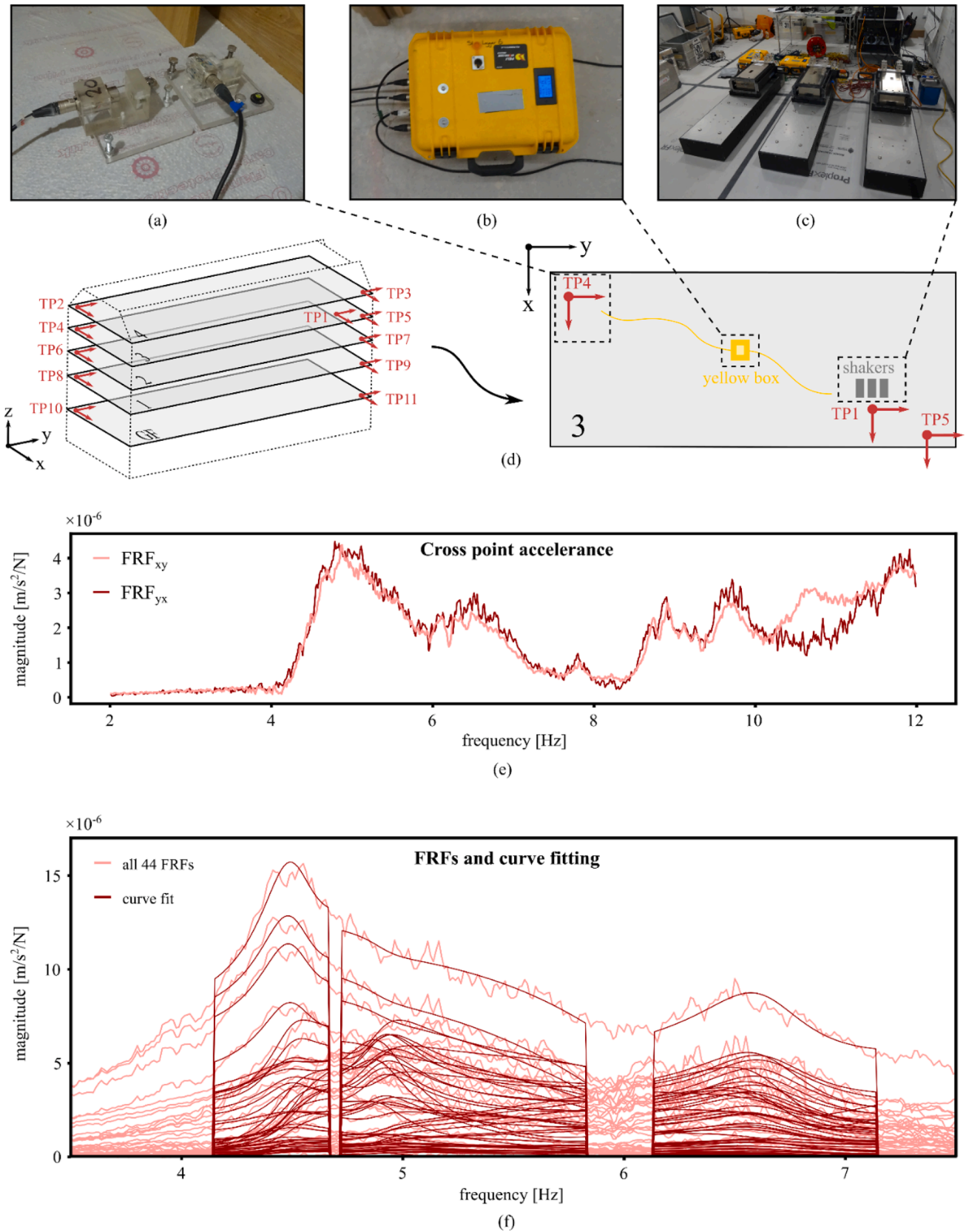


Fig. 4. Modal testing of Trinity building: (a) test point with two uniaxial accelerometers, (b) OXCO-based data logger needed for synchronisation of the sensors, (c) three electrodynamic shakers located on the third floor, (d) experimental setup with locations of the sensors, (e) reciprocity check, and (f) all FRFs with curve fitting.

Table 2
Modal properties estimated by modal testing and the initial FE model.

Mode	Experiments		Initial FE model	
	Frequency	Damping ratio	Frequency	MAC
1	4.48 Hz	4.1%	4.02 Hz	0.45
2	4.90 Hz	3.0%	4.98 Hz	0.72
3	6.38 Hz	2.9%	7.10 Hz	0.87

is the height of the building. Compared to such simplistic estimation based solely on the height of the building, the initial FE model provides greater reliability. Even though this initial FE model is suitable for estimating fundamental frequency for the purpose of checking the current comfort criteria, it also demonstrates some level of modelling error. A good indicator of that is the first MAC value which is lower than the desired minimum of 0.9. Another one is the fact that the first natural frequency is underestimated, whereas the third is overestimated. Hence, the discrepancy may not be solved only by scaling the overall stiffness or mass but indicates the need for altering their distribution.

One of the aims of this paper is to find where the modelling error of the initial model originates from. The most obvious sources could be the misestimated stiffness (or mass) of the three main structural systems (concrete GF, timber superstructure and masonry cladding) and the connections between them. Some other potential sources may be the absence of modelling of the adjacent abutting buildings, compliance of the foundation or stiffness of the screed. To test them, changes were made to the model in order to improve the matching of the natural frequencies and mode shapes. The following procedure has been used:

1. **Identify the influential parameters through one-at-a-time sensitivity analysis, observing the sensitivity of natural frequencies and MAC values.** While doing this improving the mode shapes was a struggle. More than 40 different parameters were considered, many of them had a significant effect on natural frequencies, but hardly any effect on the MAC values, see Fig. 7. When tuning parameters within the reasonable range only a few improved MAC values for more than 0.1.
2. **Perform model updating with different sets of updating parameters.** Parameters sometimes interact with each other, therefore the combined effect of simultaneous change of multiple parameters might be greater than that of each individual parameter. Model updating searches for the optimum parameter values to improve the matching of the model and experiments.

Due to the difficulty of improving mode shape matching, the parameters that achieve that were considered the most probable source of the initial modelling error. The results of this analysis are presented in the following sections.

5.2. Parameter exploration

An extensive one-at-a-time sensitivity analysis was carried out to find the influential FE modelling parameters. Its results are presented in Fig. 7. Altogether, 43 stiffness and mass parameters were considered. They were categorized into 6 groups based on the relevant part of the building.

Most of the parameters were defined as a continuous variable altering a material property or mass of a certain building component

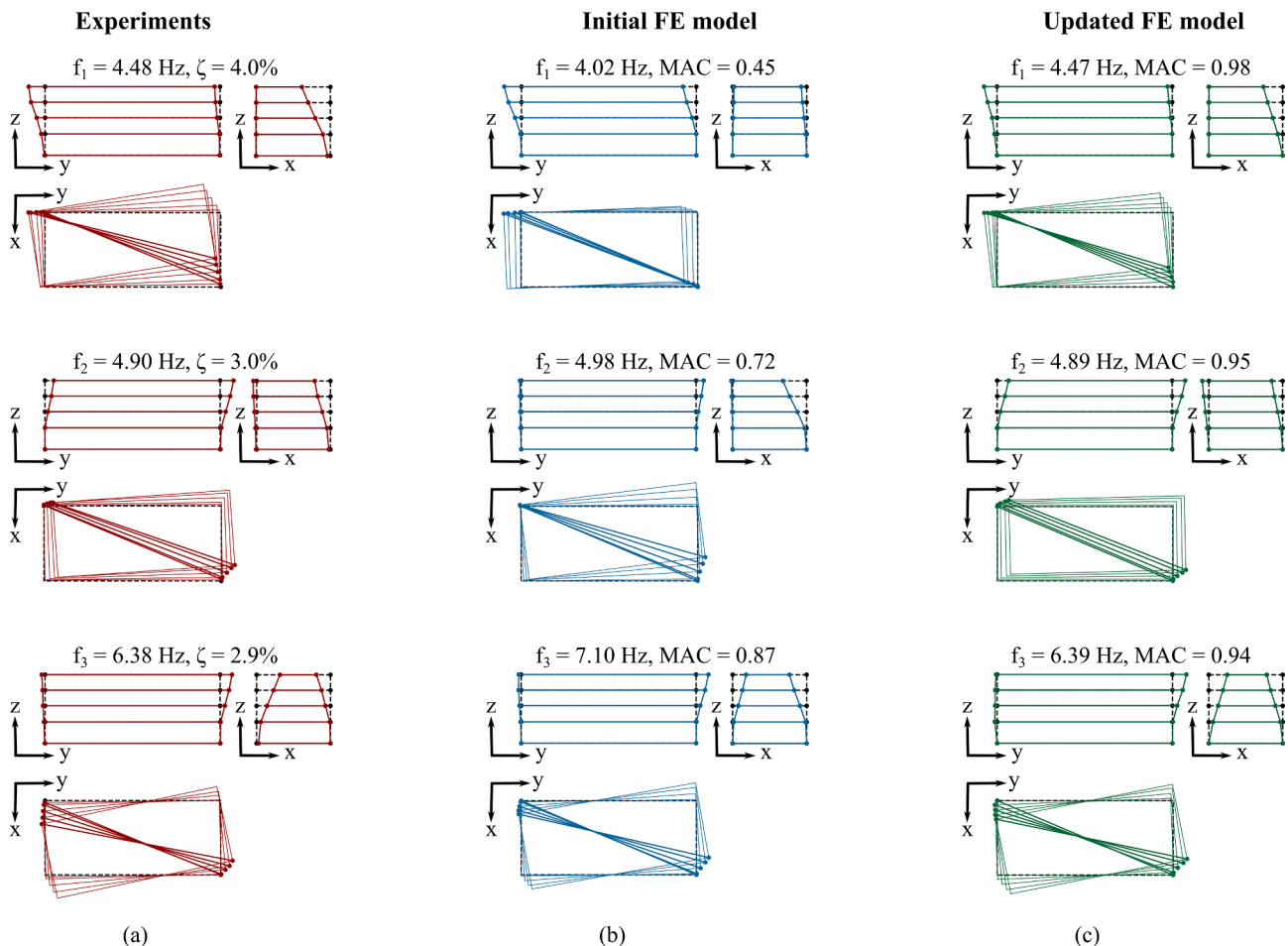


Fig. 5. Modal properties obtained from (a) experiments, (b) the initial, and (c) the updated FE model (AFG).

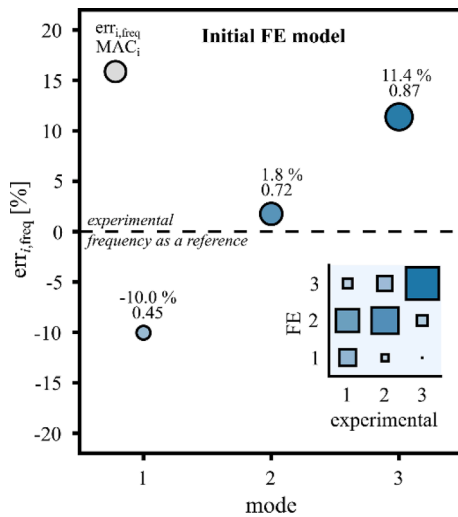


Fig. 6. FMAC plot of the initial FE model. Error $err_{i,freq}$ and MAC_i are calculated according to Eqs. (1) and (2), respectively. FMAC is enhanced with the MAC matrix in the bottom right corner.

from its initial value. Each parameter was varied within the predefined range, while all other parameters remained at their initial value. The consequent changes of the natural frequencies and MAC values were observed. The highest and lowest values of each quantity of interest were used to determine the sensitivities. The sensitivities of natural frequencies were presented as their relative change from the initial model and the sensitivities of MAC values were presented as the range between the highest and lowest MAC values achieved by varying the parameter. This definition of sensitivity is highly dependent on the width of the parameter's range of values. They were fairly wide and their choice reflected the parameters' estimated uncertainty (e.g. greater uncertainty for stiffness than mass was assumed).

There were some exceptions to how parameters were defined. Parameters 1 and 28 were not continuous variables. They were binary variables, meaning that the feature (masonry cladding for parameter 1 and screed for parameter 28) was either modelled or not modelled. Parameters 41 to 43 presented modelling features that were not included in the initial model. Parameters 41 and 42 modelled the effects of the two adjacent abutting buildings on the South-West side of the building, which were implemented as elastic supports with stiffnesses k_A (parameter 41) and k_B (parameter 42). In the initial model, these external walls were unconstrained. Elastic support with stiffness k_F (parameter 43) modelled the compliance of the foundation, which was assumed to be rigid in the initial model. All three elastic supports acted in the normal direction to the defined areas (see Fig. 8).

The purpose of the sensitivity analysis was to find parameters that may cumulatively close the gap between experiments and the model. Regarding natural frequencies, the initial FE model made up to 11 % error for the first three modes. The results of the sensitivity analysis show that many of the observed parameters may reduce a significant part of this error. In contrast, only two parameters (41 and 43) can improve MAC values significantly. Consequently, those two parameters pinpoint the most likely source of modelling error of the initial FE model and are selected as the updating parameters. However, as these two parameters alone might not sufficiently improve the model, others are also considered, based on the results in Fig. 7.

Considering a modelling approach for masonry cladding, there are two extreme scenarios – cladding and CLT superstructure are (1) completely uncoupled or (2) rigidly coupled. Since the as-built stiffness of ties between the cladding and CLT is unknown, it is practically impossible to predict how the two systems behave in a case of small amplitude vibrations. The sensitivity analysis showed that there is a significant difference in natural frequencies between those two

scenarios (parameter 1). MAC values could suggest which modelling approach is better, however, they do not significantly differ for the two modelling approaches. Therefore, the modelling of masonry cladding is used in model updating for further investigation.

A very similar case is with the modelling of the screed (parameter 28). In the initial FE model, the stiffness of the screed was neglected and only mass was considered. The assumption of the additional 65 mm thick layer of concrete, perfectly bonded to the CLT floor slabs, caused a considerable increase in the first three natural frequencies of up to 13%. However, understanding the influence of a more complex floor system (which is described in Section 2) is not straightforward. Sound insulation panels could offer a flexible connection with floor slabs, but the connection with wood flooring and walls might be more rigid. To understand its influence better, this parameter is also included in the model updating.

CLT structure takes up the majority of the building's volume. From the six constants of the orthotropic material model for CLT panels (parameters 5 to 10), only elastic modulus parallel to the grain E_1 and in-plane shear modulus G_{12} have a significant influence on natural frequencies and mode shapes. The majority of the sensitivity to G_{12} comes from its effect on the walls (parameter 11), rather than on the slabs (parameter 12). Moreover, elastic modulus E_1 of the vertical layers of the CLT walls (parameter 13) has a much greater influence on the natural frequencies than E_1 of the horizontal layers (parameter 14). In a previous study [20], the elastic modulus of the vertical layers was identified as a key parameter in the model updating of a seven-storey CLT building to improve MAC values. However, in the current study, its influence is not as significant, which can be attributed to the hybrid building's less slender structure, where more shear is engaged (as opposed to bending). Lastly, varying E_1 and G_{12} in an individual floor slab does not show a significant influence on natural frequencies or mode shapes (parameters 15 to 22). Even though overall in-plane shear modulus G_{12} (parameter 7) is the most influential of all the parameters attributed to the stiffness of CLT, in-plane shear modulus of CLT walls (parameter 11) is chosen for model updating. Such selection makes a separation between this parameter acting on walls and screed acting on floor slabs. It should be pointed out that besides the uncertainty of material properties, the parameter captures the effect of other contributions to the overall shear stiffness of the wall system (plasterboards with metal framing, partition walls, and connections between panels).

Finally, proportionally scaling the total mass of the building (parameter 29) does – not surprisingly – significantly change the natural frequencies. However, mode shapes are not influenced by such change of mass, not even after a slight redistribution of mass between the storeys (parameters 30 to 40). Due to the large influence of the total mass of the building (parameter 29), it is considered in model updating.

Altogether, six modelling features were selected for further investigation:

- Stiffness k_A of elastic support modelling the effect of the abutting building (parameter 41).
- Stiffness k_F of elastic support modelling compliance of foundation (parameter 43).
- Factor k_G multiplying in-plane shear modulus of CLT walls (parameter 11).
- Including (or excluding) the screed in the model (parameter 28).
- Including (or excluding) the masonry cladding in the model (parameter 1).
- The total mass of the building (parameter 29).

5.3. Model updating

One of the objectives of this research is to find where the FE modelling error stems from. The sensitivity analysis presented in the previous section indicated which parameters are most influential and may potentially improve the model. However, the results of the one-at-a-

group	#	Parameter description	Range of values		Sensitivity of natural frequencies*						Sensitivity of MAC values**			
			relative to initial model		1 st eigenfrequency	2 nd eigenfrequency	3 rd eigenfrequency	MAC ₁	MAC ₂	MAC ₃				
Masonry	1.	masonry clad.	not incl.	incl.	-7.2%	-5.3%	-15%		0.08	0.06	0.09			
	2.	density	-20%	+20%	<1%	<1%	<1%		<0.03	<0.03	<0.03			
	3.	E	-50%	+50%	-1.3%	+1.1%	-1.5%	+1.1%	-1.0%	+0.7%	<0.03	<0.03	<0.03	
	4.	G	-50%	+50%	-2.1%	+1.3%	-1.8%	+1.1%	-4.6%	+2.7%	<0.03	<0.03	0.10	
CLT (general)	5.	E ₁	-50%	+50%	-6.5%	+4.3%	-4.7%	+2.9%	-5.6%	+3.2%	0.06	<0.03	0.06	
	6.	E ₂	-50%	+50%	<1%	<1%	<1%	<1%	<1%	<1%	<0.03	<0.03	<0.03	
	7.	G ₁₂	-50%	+50%	-11%	+7.5%	-11%	+7.6%	-11%	+7.3%	<0.03	0.04	0.10	
	8.	G ₁₃	-50%	+50%	<1%	<1%	<1%	<1%	<1%	<1%	<0.03	<0.03	<0.03	
	9.	G ₂₃	-50%	+50%	<1%	<1%	<1%	<1%	<1%	<1%	<0.03	<0.03	<0.03	
	10.	ν ₁₂	0.2	0.4	<1%	<1%	<1%	<1%	<1%	<1%	<0.03	<0.03	<0.03	
	11.	G ₁₂ (walls)	-50%	+50%	-10%	+6.9%	-11%	+7.4%	-6.7%	+5.0%	<0.03	<0.03	<0.03	
	12.	G ₁₂ (slabs)	-50%	+50%	<1%	<1%	-4.2%	+2.3%			<0.03	<0.03	0.08	
	13.	E ₁ (vertical)	-50%	+50%	-4.8%	+3.2%	-3.8%	+2.3%	-2.5%	+1.6%	<0.03	<0.03	<0.03	
	14.	E ₁ (horizontal)	-50%	+50%	<1%	<1%	<1%	<1%	<1%	<1%	<0.03	<0.03	<0.03	
CLT (local)	15.	E ₁ (slab 2)	-50%	+50%	<1%	<1%	<1%	<1%	<1%	<1%	<0.03	<0.03	<0.03	
	16.	G ₁₂ (slab 2)	-50%	+50%	<1%	<1%	<1%	<1%	<1%	<1%	<0.03	<0.03	<0.03	
	17.	E ₁ (slab 3)	-50%	+50%	<1%	<1%	<1%	<1%	<1%	<1%	<0.03	<0.03	<0.03	
	18.	G ₁₂ (slab 3)	-50%	+50%	<1%	<1%	<1%	<1%	<1%	<1%	<0.03	<0.03	<0.03	
	19.	E ₁ (slab 4)	-50%	+50%	<1%	<1%	<1%	<1%	<1%	<1%	<0.03	<0.03	<0.03	
	20.	G ₁₂ (slab 4)	-50%	+50%	<1%	<1%	-1.5%	+1.0%			<0.03	<0.03	0.03	
	21.	E ₁ (flat roof)	-50%	+50%	<1%	<1%	<1%	<1%	<1%	<1%	<0.03	<0.03	<0.03	
	22.	G ₁₂ (flat roof)	-50%	+50%	<1%	<1%	-1.5%	+0.9%			<0.03	<0.03	<0.03	
	23.	E	-50%	+50%	-3.7%	+1.7%	-5.8%	+3.2%	-3.1%	+1.8%	0.13	0.08	<0.03	
	24.	E (walls)	-50%	+50%	-2.0%	+1.0%	-2.9%	+1.4%	-2.0%	+1.0%	0.09	0.06	<0.03	
Concrete	25.	E (columns)	-50%	+50%	<1%	<1%	<1%	<1%	<1%	<1%	<0.03	<0.03	<0.03	
	26.	E (slab GF)	-50%	+50%	<1%	<1%	<1%	<1%	<1%	<1%	<0.03	<0.03	<0.03	
	27.	E (slab 1)	-50%	+50%	-1.5%	+0.8%	-2.2%	+1.3%	-1.1%	+0.7%	<0.03	<0.03	<0.03	
	28.	screed	not incl.	incl.		+7.4%		+4.6%		+13%	0.05	<0.03	0.10	
	29.	total mass	-20%	+20%	-6.3%	+7.8%	-6.2%	+7.7%	-6.3%	+7.7%	<0.03	<0.03	<0.03	
	30.	mass (slab GF)	-20%	+20%	<1%	<1%	<1%	<1%	<1%	<1%	<0.03	<0.03	<0.03	
	31.	mass (walls GF)	-20%	+20%	<1%	<1%	<1%	<1%	<1%	<1%	<0.03	<0.03	<0.03	
	32.	mass (slab 1)	-20%	+20%	<1%	<1%	<1%	<1%	<1%	<1%	<0.03	<0.03	<0.03	
	33.	mass (walls 1)	-20%	+20%	<1%	<1%	<1%	<1%	<1%	<1%	<0.03	<0.03	<0.03	
	34.	mass (slab 2)	-20%	+20%	<1%	<1%	<1%	<1%	<1%	<1%	<0.03	<0.03	<0.03	
Distributed mass	35.	mass (walls 2)	-20%	+20%	<1%	<1%	<1%	<1%	<1%	<1%	<0.03	<0.03	<0.03	
	36.	mass (slab 3)	-20%	+20%	<1%	<1%	<1%	<1%	<1%	<1%	<0.03	<0.03	<0.03	
	37.	mass (walls 3)	-20%	+20%	<1%	<1%	<1%	<1%	<1%	<1%	<0.03	<0.03	<0.03	
	38.	mass (slab 4)	-20%	+20%	-1.6%	+1.7%	-1.5%	+1.6%	-1.5%	+1.5%	<0.03	<0.03	<0.03	
	39.	mass (walls 4)	-20%	+20%	<1%	<1%	<1%	<1%	<1%	<1%	<0.03	<0.03	<0.03	
	40.	mass (roof)	-20%	+20%	-1.9%	+2.0%	-2.1%	+2.2%	-2.2%	+2.2%	<0.03	<0.03	<0.03	
	Elastic support	41.	k _A [MN/m ³]	not incl.	10 ²		+26%		+23%		+1.4%	0.49	0.50	<0.03
		42.	k _B [MN/m ²]	not incl.	10 ²	<1%	<1%	<1%	<1%	+5.7%		<0.03	<0.03	0.07
		43.	k _F [MN/m ²]	1	rigid	-59%	-55%	-54%				0.53	0.85	0.08

* Change of natural frequencies when a parameter is increased (or decreased) by a certain margin while other assumptions remain unchanged. The colour of the box denotes whether a parameter increases or decreases natural frequency.
 ** Range of MAC values when a parameter is changed within its range while other assumptions remain unchanged. In contrast to natural frequencies, it cannot be determined whether a parameter increases or decreases MAC values as they don't behave monotonously.

Fig. 7. Results of one-at-a-time sensitivity analysis.

time sensitivity analysis itself do not uncover the sources of the error. To that end, model updating was carried out. The problem in model updating is when too many parameters are included it might lead to misinterpretation of the updated parameters. Therefore, a minimal set of parameters that updates the model well enough was sought. As a criterion of a well-matched model, the following conditions were used:

$$\text{each } MAC_i > 0.9 \text{ and each } |\text{err}_{i,\text{freq}}| < 1\% \quad (3)$$

Due to potential measurement and modal identification errors, it is unnecessary to aim for better matching. Each model satisfying these conditions will be included in the final analysis of the results to estimate the confidence intervals of the updated parameter values.

Multi-objective optimization algorithm, NSGA-II [46], was used for

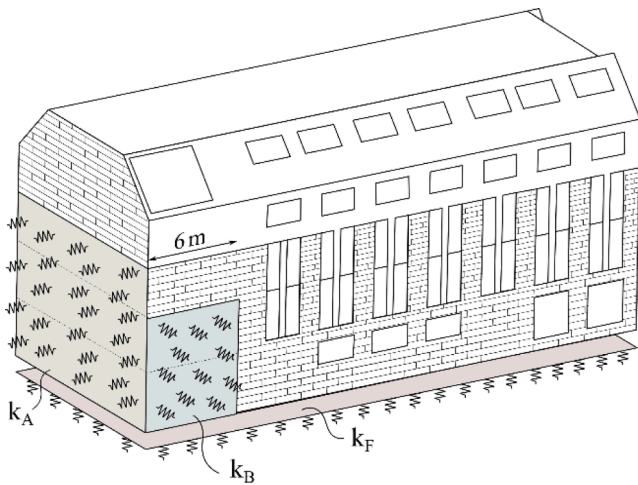


Fig. 8. Defining areas of the three elastic supports modelling effects of the two adjacent abutting buildings and the foundation. Parameters k_A , k_B , and k_F define their stiffness.

model updating. Two objective functions were defined as a measure of how well the FE model matches the experiment with regard to mode shapes:

$$\delta_{\text{MAC}} = \sum_{i=1}^3 (1 - \text{MAC}_i)^2, \quad (4)$$

and natural frequencies

$$\delta_{\text{freq}} = \sum_{i=1}^3 (\text{err}_{i,\text{freq}})^2. \quad (5)$$

To minimize the objective functions, an optimization algorithm was implemented with a help of an open-source library *pymoo* [47]. The NSGA-II multi-objective algorithm is Pareto-based optimization where the weights of the objective functions are not initially given. In the end, not one particular optimum solution is obtained, but rather a set of Pareto-optimal solutions (also called Pareto front). This essentially means that until additional information is given (e.g. weights of objective functions) all of those solutions are equally good alternatives [46]. Making a trade-off between the objective functions is then left to the decision-maker. There are a few algorithmic approaches to this decision-making, the simplest being just choosing the weight for each objective function [46]. In our case, weights of 1 and 100 are ascribed to objective functions δ_{MAC} and δ_{freq} , respectively, in order to equalize their effects according to the criteria from Eq. (3) (i.e. a model that barely satisfies these criteria should have both objective functions of the same value).

Nine iterations of model updating were carried out. In the first four iterations different combinations of the three modelling parameters – k_A , k_F , and k_G – were used. In the next two iterations, modelling assumptions about screed and masonry cladding are tested. Lastly, three iterations of updating the models with varying total building mass are carried out. The updated models of each iteration are presented with FMAC plots [48] in Fig. 9. They show how well the three modes are matching the experiments, according to the measures from Eqs. (1) and (2). For each model updating iteration, modelling assumptions and updated parameters are denoted above the plot. To avoid limiting strict assumptions for the bounds initially, the ranges of parameter values were wide enough that the updated values were not close to their bounds (otherwise the updating was repeated). In such a way, potential information about the modelling error is not lost. Instead, the unreasonable updated parameter values are critically addressed in the analysis of the results.

In each of the first three iterations, only two updating parameters were used, however, none of the updated models satisfied the criteria from Eq. (3). Updated model AF (Fig. 9a) was the closest, but the second

mode was matched with the experiments by a MAC value of only 0.78. Updated model FG (Fig. 9b) had errors of the first and the third natural frequencies –3.3% and 2.5%, respectively. In addition, the updated value of k_G suggested an unreasonable fivefold increase of shear stiffness of the CLT walls. Updated model AG (Fig. 9c) was matched even worse – with $\text{MAC}_2 = 0.56$ and $\text{err}_{3,\text{freq}} = 4.5\%$. When all three modelling parameters – k_A , k_F , and k_G – were used, the updating resulted in a far better solution (Fig. 9d). Updated model AFG matched with the experiments with all three MAC values higher than 0.9 and errors of the first three natural frequencies less or equal to 0.2%.

Next, the two assumptions about modelling screed and masonry cladding are tested. Updated model $\text{AFG}^{+\text{screed}}$ (Fig. 9e) was achieved by updating the same three parameters as in AFG model, but adding a stiffness of 65 mm thick layer of screed to the model. Its matching with the experiments is observed to be slightly worse, mainly due to the error of the third natural frequency increasing to almost 2%. However, the worsening of the model is not significant enough to conclude that the screed should not be modelled. Then, updating of the model with the masonry cladding excluded from the model was carried out, resulting in model $\text{AFG}^{-\text{masonry}}$ (Fig. 9f). This model investigates the possibility that the masonry cladding and the load-bearing structure behave as two uncoupled systems under the testing conditions. Even though the updated model satisfies the criteria from Eq. (3) and is comparable to model AFG, this scenario is dismissed. As a consequence of removing the masonry cladding from the model, the updated value of parameter k_G suggests shear stiffness of CLT walls to be almost four times higher than initially anticipated – a value that can hardly be justified.

Finally, the uncertainty of the total building mass is considered in the last three iterations. Model updating is carried out as in AFG, but the total building mass has been proportionally decreased to 80% (Fig. 9g), 90% (Fig. 9h) or increased to 110% (Fig. 9i) of the initial mass. It was assumed that the initial mass is more likely to be overestimated than underestimated since they were calculated for the ultimate limit state check. All three iterations resulted in the models that satisfy the criteria from Eq. (3). Expectedly, when mass is changed, updated stiffness parameters change as well (see Fig. 10). The confidence interval of a parameter in each iteration is obtained from the set of models that satisfy the criteria from Eq. (3). Due to unreasonably high values of k_G , the scenario with the assumption of 110% total mass is dismissed. The remaining three ($\text{AFG}^{80\% \text{mass}}$, $\text{AFG}^{90\% \text{mass}}$, and AFG) are used to determine range of updated values. This is done by taking the lowest and highest parameter values from the set of models satisfying the criteria from Eq. (3). The updated parameter ranges are presented in Table 3.

To give more meaning to the updated parameter values, the impact of each parameter on the stiffness of the model has been estimated (see Table 3). For example, adding elastic support modelling the influence of the adjacent abutting building with the low estimate of the updated stiffness $k_A = 4.5 \text{ MN/m}^3$ increases the stiffness of the initial FE model in the y direction by 9%, or when using the high estimate ($k_A = 17.5 \text{ MN/m}^3$), the stiffness of the initial FE model in the y direction increases by 21%. Parameter stiffness k_A has no effect in the x direction. Similarly, parameter k_F decreases stiffness in the x direction between 26% and 35%, and in the y direction between 7% and 10%. Lastly, the updated parameter values of k_G increase stiffness of the initial FE model by at least 10% and 12% in the x and y directions, respectively. The stiffness has been calculated by applying unit displacement at the fourth floor in either x or y direction and reading the resulting reaction force in that direction.

Including mass and stiffness as parameters in model updating requires a critical examination of the results. As a quality check, one can compare the static stiffness of the FE model with the experimentally obtained one. To estimate static stiffness with the FE model, a unit displacement was applied to the area on the 3rd floor, where the shaker was placed during the testing. A static stiffness is calculated as a resultant reaction force on the same area and in the direction of the applied

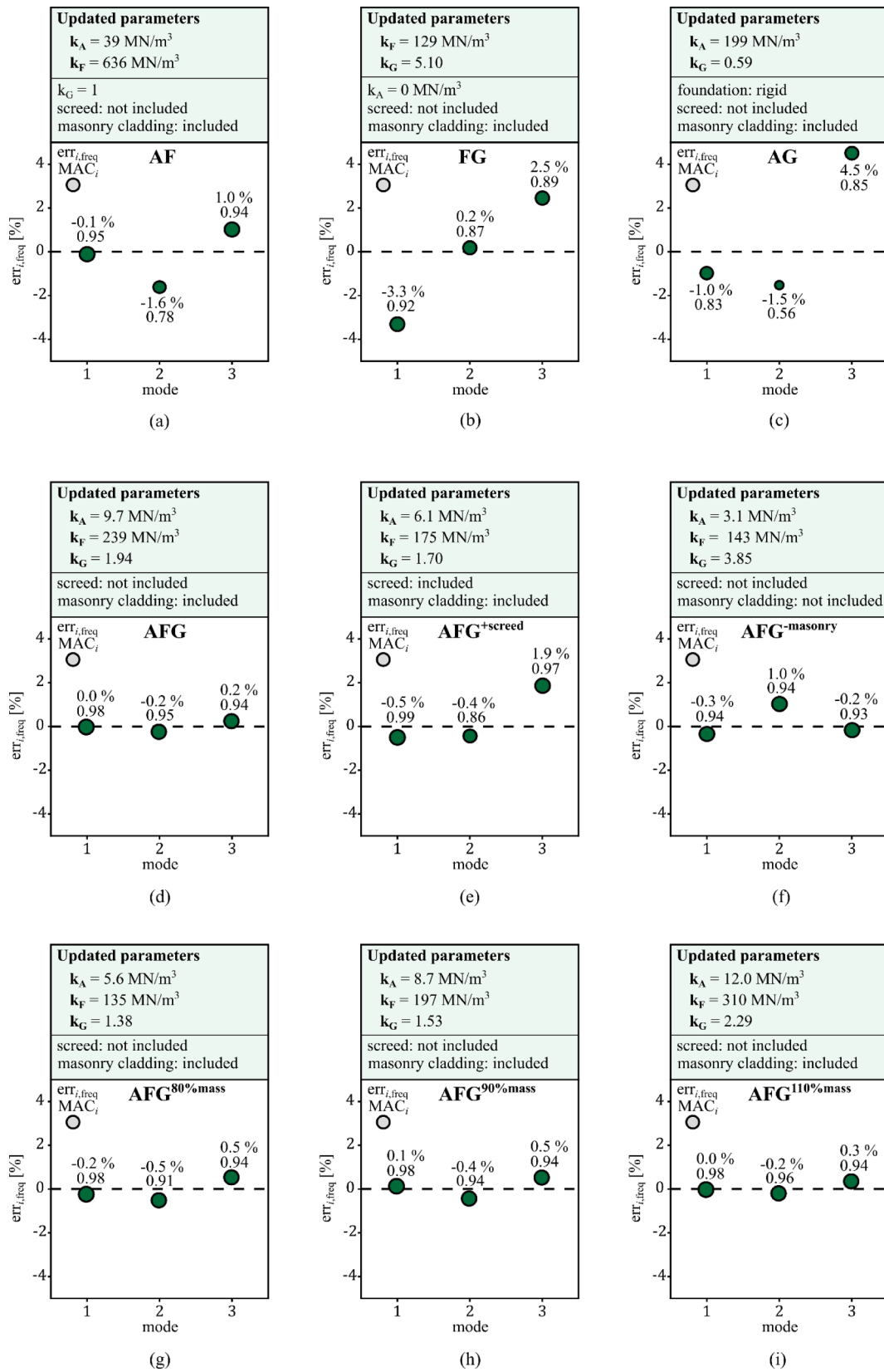


Fig. 9. FMAC plots of nine updated models that were obtained with different settings.

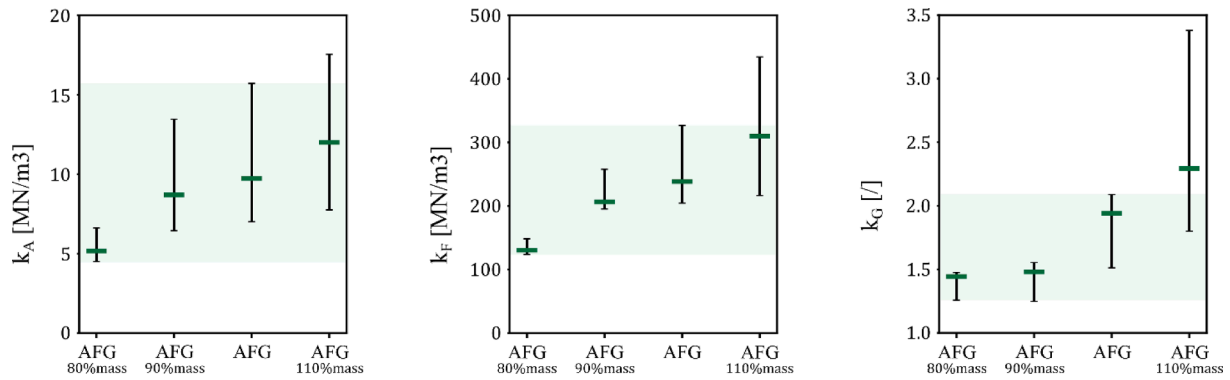


Fig. 10. Updated parameter values depending on the mass assumption.

Table 3
Range of updated parameter values.

Parameter	Range of updated values		Impact on the initial FE model stiffness	
			x direction	y direction
k_A [MN/m ³]	Low estimate	4.5	0%	+9%
	High estimate	15.7	0%	+21%
k_F [MN/m ³]	Low estimate	125	-26%	-7%
	High estimate	327	-35%	-10%
k_G [/]	Low estimate	1.25	+10%	+12%
	High estimate	2.09	+35%	+40%

unit displacement. Experimental static stiffness is not explicitly calculated due to the low signal-to-noise ratio in the low-frequency range. Instead, static FE model compliance is calculated as an inverse of the static stiffness and compared with the experimental receptance, shown in Fig. 11. Both, static compliance in the directions x (Fig. 11a) and y (Fig. 11b), fit well with the experimental point receptances. Compliance in the x direction is practically unchanged after the updating (AFG), whereas compliance in the y direction seems to be slightly improved after the updating compared with the compliance of the initial model.

5.4. Discussion

The two most important sources of modelling error found in this analysis both have a large impact on the natural frequencies of the building, however, their effects are opposing. Foundation makes the structure less stiff, whereas the abutting building offers support and thus

making it stiffer. A good prediction of natural frequencies by the initial model, therefore, seems more of a fortunate consequence of the two modelling errors cancelling out.

The updated vertical foundation stiffness suggests that the stiffness of the building is reduced by at least 26% and 7% in the x and y directions, respectively, due to the compliance of the foundation. The updated value of k_F can be compared to the typical values of the subgrade reaction coefficient, which is defined as the ratio of the pressure under a loaded slab and the settlement produced by the load [49]. The value of the coefficient is strongly influenced by the type of subgrade. In the formation level, medium dense to very dense sandy gravel and stiff clay are reported. Typical values of subgrade reaction coefficient are 10–25, 25–125 and 125–375 MN/m³ for stiff clay, medium dense sand and dense sand, respectively [50]. Foundation being modelled as a linear elastic support is a considerable simplification, but those values (even in a large range) affirm that the updated foundation stiffness is of the right order of magnitude. Similarly, a slight softening effect of the foundation was found previously [20].

Even though the abutting building is designed independently with no lateral load-bearing connections, it has a significant influence on the modal properties (updated value of k_A suggests at least a 9% increase of the stiffness in the direction of the abutting building). Since there is also masonry cladding between the two buildings, this furthermore suggests that the connections between the CLT and masonry cladding do not behave as uncoupled, despite the gap in the ties allowing for vertical differential movement. The masonry cladding seemingly provided a significant increase in the natural frequencies.

The updated value of k_G suggests at least 25% higher (but very likely even more) in-plane shear stiffness of the CLT walls than anticipated

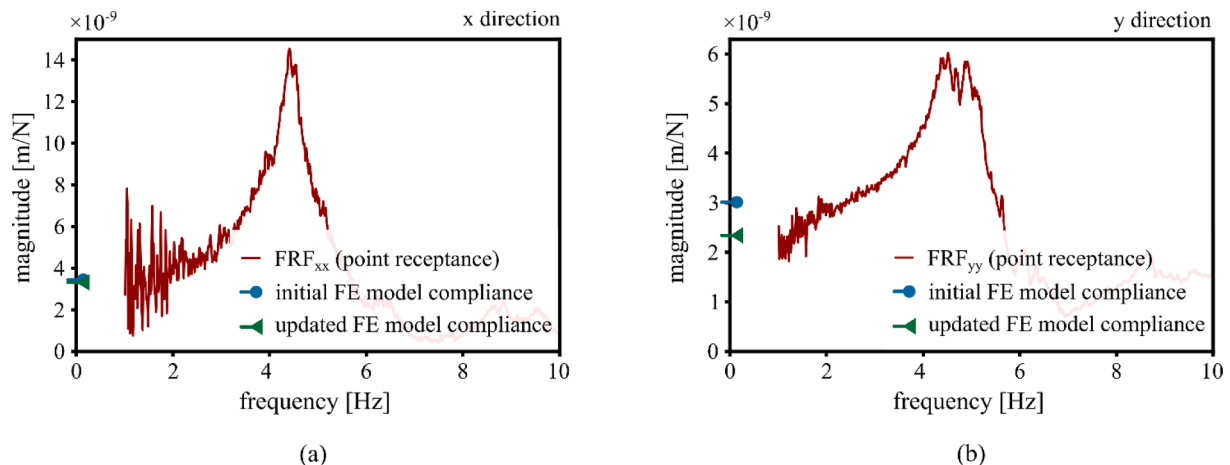


Fig. 11. Direct point receptance in test point TP1 (a) in the x direction and (b) in the y direction. For comparison, the static compliances of the initial and the updated FE model are shown.

from the shear modulus of CLT given by its producer. This would mean the in-plane shear modulus of CLT to be at least 625 GPa. That is possible, however, it could also be that the non-structural parts of timber walls actually contribute to the higher stiffness. In fact, two layers of plasterboard (one on each side of the wall) with metal framing and insulation have roughly the same mass as the typical indoor CLT wall with a thickness of 120 mm. The conclusion of initially underestimated stiffness goes in line with the results of the previous study [20], where a 60% increase in the shear stiffness of CLT walls was found.

In the initial FE model, an assumption of rigid connections was adopted. All successfully updated models suggested that the building's shear stiffness is even higher than initially estimated, despite allowing wide ranges of parameter values. It seems unlikely that steel connections between CLT panels significantly reduced the stiffness of the building in small amplitude vibration.

6. Conclusion

A 5-storey hybrid timber-concrete building has been studied. An FRF-based forced vibration testing was performed on this 2 000 t building to obtain 3 modes of vibration, their natural frequencies were 4.48 Hz, 4.90 Hz, 6.38 Hz and their damping ratios 4.0%, 3.0%, 2.9%, respectively.

A detailed FE model developed based on best engineering judgement before the testing predicted the natural frequencies with up to slightly more than 11% error. Mode shape matching was not as satisfactory with the MAC value for the first mode below 0.5. After model updating natural frequencies were matched to the experiments with an error lower than 1% and MAC values above 0.9.

The following case-specific conclusions have been drawn about necessary assumptions for accurate modelling of modal properties:

- The usual assumption of a rigid foundation is not correct.
- The adjacent abutting building offers significant support to the studied building, hence it should not be neglected.
- The masonry cladding seems to be well connected horizontally with the CLT structure, despite the allowed vertical differential movement in steel ties. Therefore, the cladding should be included in the modelling.
- The shear stiffness of the CLT walls turns out to be more than 25% higher than anticipated based on the in-plane shear modulus proposed by the producer of the CLT panels. It is likely that non-structural elements contribute to the higher stiffness of the building.

Due to the complexity of the building and a large number of uncertain building elements, it was difficult to pinpoint more precisely where the modelling error lies. To obtain more information from such model updating, it is important to keep uncertainties of input parameters as low as possible (mainly in-plane shear modulus of the CLT panels, mass, and stiffness of the foundation).

The study showed that mode shape matching was more difficult to improve than the matching of natural frequencies. For this reason, increasing the number of measured degrees of freedom and the number of identified (and updated) modes seems beneficial. Another improvement would be to perform modal testing in several stages during the construction. For each, an FE model should be built and the newly added modelling features updated.

CRedit authorship contribution statement

Blaž Kurent: Methodology, Investigation, Formal analysis, Visualization, Writing – original draft, Writing – review & editing. **Wai Kei Ao:** Methodology, Investigation, Formal analysis. **Aleksandar Pavic:** Conceptualization, Writing – original draft, Writing – review & editing, Supervision. **Fernando Pérez:** Resources, Data curation. **Boštjan Brank:** Conceptualization, Supervision.

Declaration of Competing Interest

The authors declare that they have no known competing financial interests or personal relationships that could have appeared to influence the work reported in this paper.

Data availability

The authors do not have permission to share data.

Acknowledgements

The support of ERA-NET Cofund Forest Value (DynaTTB project) and the corresponding funding bodies (Ministry of Education, Science and Sport of the Republic of Slovenia for BK and BB, and Forestry Commission GB for AP and WKA) is gratefully acknowledged. BK and BB also acknowledge the financial support of the Slovenian Research Agency (J2-2490). We thank the design office Smith and Wallwork Ltd at Cambridge, UK, for the documentation and helpful discussions, Trinity College for letting us perform the testing and access the documentation, and Morgan Sindall for enabling and helping with the testing during the final stages of construction.

References

- [1] United Nations Environment Programme, "Global Status Report for Buildings and Construction: Towards a Zero-emission, Efficient and Resilient Buildings and Construction Sector," Nairobi, 2021.
- [2] Orr J, Drewniok MP, Walker I, Ibell T, Copping A, Emmitt S. Minimising energy in construction: Practitioners' views on material efficiency. *Resour Conserv Recycl* 2019;140:125–36.
- [3] Harris NL, Gibbs DA, Baccini A, Birdsey RA, de Bruin S, Farina M, et al. Roman-Cuesta and Saatc, "Global maps of twenty-first century forest carbon fluxes". *NatureClimate Change* 2021;11(3):234–40.
- [4] Foster RM, Reynolds TPS. Lightweighting with Timber: An Opportunity for More Sustainable Urban Densification. *J Archit Eng* 2018;24(1).
- [5] Johansson M, Linderholt A, Bolmsvik Å, Jarnerö K, Olsson J, Reynolds T. Building higher with light-weight timber structures: the effect of wind induced vibrations. In: *Proceedings of the Internoise 2015 conference*, San Francisco, US, 2015.
- [6] Edskär I, Lidelow H. Dynamic properties of cross-laminated timber and timber truss building systems. *Eng Struct* 2019;186:525–35.
- [7] Aktan AE, Brownjohn JMW. Structural identification: Opportunities and challenges. *ASCE J Struct Eng* 2013;10:1639–47.
- [8] Tulebekova S, Malo KA, Rönquist A, Nåvik P. Modeling stiffness of connections and non-structural elements for dynamic response of taller glulam timber frame buildings. *Eng Struct* 2022;261:114209.
- [9] Aloisio A, Pasca D, Tomasi R, Fragiaco M. Dynamic identification and model updating of an eight-storey CLT building. *Eng Struct* 2020;213:110593.
- [10] Reynolds T, Harris R, Chang W-S, Bregulla J, Bawcombe J. Ambient vibration tests of a cross-laminated timber building. *Proc Inst Civil Eng - Constr Mater* 2015;168(3):121–31.
- [11] Guler K, Yuksel E, Kocak A. Estimation of the Fundamental Vibration Period of Existing RC Buildings in Turkey Utilizing Ambient Vibration Records. *J Earthq Eng* 2008;12(sup2):140–50.
- [12] Soyoz S, Taciroglu E, Orakcal K, Nigbor R, Skolnik D, Luş H, et al. Ambient and Forced Vibration Testing of a Reinforced Concrete Building before and after Its Seismic Retrofitting. *J Struct Eng* 2013;139:1741–52.
- [13] Memari AM, Aghakouchak AA, Ghafory Ashtiany M, Tiv M. Full-scale dynamic testing of a steel frame building during construction. *Eng Struct* 1999;21(12):1115–27.
- [14] Steiger R, Feltrin G, Weber F, Nerbano S, Motavalli M. Experimental modal analysis of a multi-storey light-frame timber building. *Bull Earthq Eng* 2017;15:3265–91.
- [15] Ellis BR, Boughard AJ. Dynamic testing and stiffness evaluation of a six-storey timber framed building during construction. *Eng Struct* 2001;23(10):1232–42.
- [16] Reynolds T, Casagrande D, Tomasi R. Comparison of multi-storey cross-laminated timber and timber frame buildings by in situ modal analysis. *Constr Build Mater* 2016;102:1009–17.
- [17] Larsson C, Abdeljaber O, Bolmsvik Å, Dorn M. Long-term analysis of the environmental effects on the global dynamic properties of a hybrid timber-concrete building. *Eng Struct* 2022;268:114726.
- [18] Ewins DJ. *Modal Testing: Theory, Practice and Application*, Taunton. UK: Research Studies Press Ltd.; 1984.
- [19] Satake N, Suda K-I, Arakawa T, Sasaki A, Tamura Y. Damping Evaluation Using Full-Scale Data of Buildings in Japan. *J Struct Eng* 2003;129(4):440–77.
- [20] Kurent B, Brank B, Ao WK. Model updating of seven-storey cross-laminated timber building designed on frequency-response-functions-based modal testing. *Struct Infrastruct Eng* 2023;19(2):178–96.

- [21] Kurent B, Friedman N, Ao WK, Brank B. model using modal data. *Eng Struct* 2022; 266:114570.
- [22] Foster RM, Reynolds T, Ramage MH. Proposal for Defining a Tall Timber Building. *J Struct Eng* 2016;142(12):02516001.
- [23] Brank B, Damjanić FB, Perić D. On implementation of a nonlinear four node shell finite element for thin multilayered elastic shells. *Comput Mech* 1995;16(5): 341–59.
- [24] EN 1992-1-1, Eurocode 2: Design of concrete structures - Part 1-1 : General rules and rules for buildings, Brussels: European committee for Standardization (CEN), 2004.
- [25] Massivholz KLH. *European Technical Assessment ETA-06/0138 of 18.01.2021. Austrian Inst Constr Eng* 2021.
- [26] EN 1996-1-1, Eurocode 6 - Design of masonry structures - Part 1-1: General rules for reinforced and unreinforced masonry structures, Brussels: European committee for Standardization (CEN), 2005.
- [27] Ao WK, Pavic A. Discovering the dynamic properties of civil structures with frf-based and wirelessly synchronised, distributed oco high precision data loggers. In: *IMAC-XXXIX Congress*, Orlando, FL, USA, 2021.
- [28] Ao WK, Pavic V. FRF-based modal testing of horizontally swaying structures using oco synchronised wireless accelerometers for simultaneous force and vibration response measurements. In: *Proceedings of the International Conference on Structural Dynamic , EUROODYN*, Athens, Greece, 2020.
- [29] Brownjohn JWM, Au S-K, Zhu Y, Sun Z, Li B, Bassitt J, et al. Bayesian operational modal analysis of Jiangyin Yangtze River Bridge. *Mech Syst Sig Process* 2018;110 (September):210–30.
- [30] Au S-K. *Operational Modal Analysis : Modeling, Bayesian Inference, Uncertainty Laws*. Singapore: Springer; 2017.
- [31] Rainieri C, Fabbrocino G. *Operational Modal Analysis of Civil Engineering Structures*. New York: Springer; 2014.
- [32] Brownjohn JWM, Magalhaes F, Caetano E, Cunha A. Ambient vibration re-testing and operational modal analysis of the Humber Bridge. *Eng Struct* 2010;32(8): 2003–18.
- [33] Cross EJ, Koo KY, Brownjohn JWM, Worden K. Long-term monitoring and data analysis of the Tamar Bridge. *Mech Syst Sig Process* 2013;35(1–2):16–34.
- [34] Cabboi A, Magalhães F, Gentile C, Cunha Á. Automated modal identification and tracking: Application to an iron arch bridge: Automated Modal Identification and Tracking. *Struct Control Health Monit* 2017;24(1):e1854.
- [35] Rainieri C, Fabbrocino G. Automated output-only dynamic identification of civil engineering structures. *Mech Syst Sig Process* 2010;24(3):678–95.
- [36] Magalhães F, Cunha A. Explaining operational modal analysis with data from an arch bridge. *Mech Syst Sig Process* 2011;25(5):1431–50.
- [37] Ao WK, Pavic A, Kurent B, Perez F. Novel FRF-based fast modal testing of multi-storey CLT building in operation using wirelessly synchronised data loggers. *J Sound Vib* 2023;548:117551.
- [38] Dta DTA. *The dynamic test agency handbook. Dynamic Testing Agency-NAFEMS* 1994.
- [39] Honeywell International Inc., Q-flex QA-750 accelerometer, Honeywell International, Inc. Defense and Space Electronic Systems Redmond, 2020.
- [40] Japan Aviation Electronics Industry, Ltd., Mems JA-70SA accelerometers, Japan Aviation Electronics Industry, Ltd., 2021.
- [41] APS Dynamics, Aps 400 electro-seis long stroke shaker with linear ball bearings, APS Dynamics, 2022.
- [42] Allemang RJ. The modal assurance criterion - Twenty years of use and abuse. *Sound Vib* 2003;37(8):14–21.
- [43] Kozánek J. The qualification number of a complex vector. *Mech Mach Theory* 1987;22(4):391–2.
- [44] ISO 10137, Bases for design of structures—Serviceability of buildings and walkways against vibrations, Geneva: International Organization for Standardization, 2007.
- [45] EN 1991-1-4, Eurocode 1: Actions on structures Part 1-4: General actions - Wind actions, Brussels: European committee for Standardization (CEN), 2010.
- [46] Deb K, Pratap A, Agarwal S, Meyarivan T. A fast and elitist multiobjective genetic algorithm: NSGA-II. *IEEE Trans Evol Comput* 2002;6(2):182–97.
- [47] Blank KDJ. *pymoo: Multi-Objective Optimization in Python*. *IEEE Access* 2020;8: 89497–509.
- [48] Fotsch D, Ewins DJ. Further applications of the FMAC. In: *Proceedings of the International Modal Analysis Conference - IMAC*, 2001.
- [49] Terzaghi K. Evaluation of coefficients of subgrade reaction. *Geotechnique* 1955;5 (4):297–326.
- [50] Das BM. *Principles of Foundation Engineering*. 7th Edition. Stamford: Cengage Learning; 2010.